

Lagrangian statistics of mesoscale turbulence in a natural environment: The Agulhas return current

Francesco Carbone, Christian N. Gencarelli, and Ian M. Hedgecock

CNR–Institute of Atmospheric Pollution Research, CNR–IIA, U.O.S. di Rende, c/o UNICAL–Polifunzionale, 87036 Rende, Italy

(Received 8 September 2016; published 5 December 2016)

The properties of mesoscale geophysical turbulence in an oceanic environment have been investigated through the Lagrangian statistics of sea surface temperature measured by a drifting buoy within the Agulhas return current, where strong temperature mixing produces locally sharp temperature gradients. By disentangling the large-scale forcing which affects the small-scale statistics, we found that the statistical properties of intermittency are identical to those obtained from the multifractal prediction in the Lagrangian frame for the velocity trajectory. The results suggest a possible universality of turbulence scaling.

DOI: [10.1103/PhysRevE.94.063101](https://doi.org/10.1103/PhysRevE.94.063101)

Turbulence is a complex phenomenon in fluid flows characterized by the presence of high amplitude fluctuations on a broad range of dynamical spatial and temporal scales, giving rise to nontrivial scale-free relationships of statistical quantities [1–4]. Turbulence is currently investigated not only because it is an as yet unsolved problem from a theoretical point of view, but also because the properties of transport processes—namely, the mixing of passive scalars within a turbulent flow dominated by the advective action of velocity fluctuations in time and space—are of particular interest from a practical point of view (e.g., the diffusion and transport of pollutants and nutrients).

However, mesoscale turbulent fluctuations in oceanic environments have seldom been investigated experimentally due to the large scales involved.

Eddies on this scale are, however, important in oceanography, as has been shown by their interaction with tropical instability waves in the eastern tropical Pacific influence ocean biology and dynamics [5]. These eddies have an impact on heat, mass, and energy transfer; tropical instability waves also modulate the turbulent entrainment flux [6]. Variations in this flux within the El Niño–La Niña cycle can have an impact on global precipitation and temperature patterns. In the oceans, eddies on these scales are tens to a few hundred kilometers in diameter; they form as a result of strongly sheared motion and are often associated with western boundary currents. They play a crucial role in mixing passive scalar properties such as heat, salinity, and carbon, but also in the transport of contaminants and nutrients. Understanding mesoscale eddy scaling properties may provide a tool to estimate the relative importance of key oceanic physical and biological drivers [7], and an understanding of SST fluctuations and their intermittent properties may provide insight into large-scale climate phenomena and teleconnections.

Here, the Lagrangian scaling properties of the sea surface temperature (SST) measured in the Agulhas return current (ARC) have been investigated, since a Lagrangian viewpoint, that is, following the motion of an infinitesimal fluid element moving with the local instantaneous flow, is conceptually natural to describe turbulent transport [8].

The Agulhas current [9] is the western boundary current of the Southern Indian Ocean, flowing southwards along the East coast of Africa between 27 and 40°S. When it reaches the southern tip of the African continental shelf, most of the flow turns back on itself, and becomes the Agulhas return current

rejoining the Indian Ocean gyre. Part of the Agulhas current feeds into the Benguela current to the west of Africa, often in the form of filaments or rings, feeding warm, salty water into the South Atlantic. This so-called Agulhas Leakage has an important role in global ocean circulation and climate [10].

The Oceans Climate Station Project [11] run by the Pacific Marine Environmental Laboratory of the National Oceanic and Atmospheric Administration deploys moored buoys to measure meteorological and oceanic variables at strategic points in the world’s oceans. One, located in the ARC, nominally at 38.5°S, 30.0°E, is a slack line mooring with a watch circle radius of 3.5 km (Fig. 1). This buoy was deployed on 30 November 2010, however, due to unexpectedly strong deep currents, it broke free on 16 January 2011, and drifted over 1000 nautical miles before being recovered on 9 March 2011 [12]. The daily averaged position of the buoy during this period is superimposed on Fig. 1 (black dots). Whilst free from its mooring, the length scales of the eddies mean that the buoy was moving noninertially. The buoy made continuous SST measurements at $\Delta t = 600$ s.

Transport by ocean currents is a controlling factor in the distribution of water mass properties on a broad range of scales, from ocean basin scale (thousands of kilometers) to the microscale (centimeters); Lagrangian measurements are particularly suitable for the study of transport processes since they move with the currents following the motion of water parcels, at least over large scale and mesoscales [13]. The standard procedure used in order to obtain information about oceanographic quantities (SST, salinity, etc.) consists of deploying fixed or drifting buoys. Drifters are free to move on the ocean surface and are transported by surface currents. Due to the strong current and the scales involved in the fluid velocity of the ARC the buoy can be considered as a 2D Lagrangian particle transported on the surface by the oceanic eddies [14–16]. The temperature (heat content of the ARC) can be considered a passive tracer because it has negligible feedback on the scale of the flow anomalies within the mesoscale eddies of the ARC.

An analogy can be made between a surface drifter and particle dispersion in the scaling of the mean square interparticle distance ($\langle \Delta \mathcal{R}^2(t) \rangle$) [$\Delta \mathcal{R}(t) = \mathcal{R}(t) - \mathcal{R}(0)$], where $\mathcal{R}(t)$ represents the Lagrangian trajectory of a particle advected by a prescribed incompressible velocity field. For a single particle, when the Lagrangian correlation time (τ^*) is finite ($t \gg \tau^*$), an effective diffusive regime arises: $\langle \Delta \mathcal{R}^2(t) \rangle = 2\langle \mathbf{v}^2 \rangle t \tau^*$ [17].

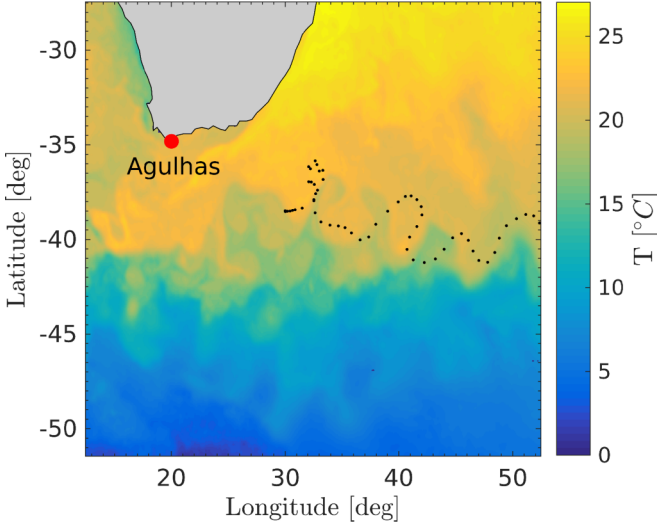


FIG. 1. A snapshot of the SST taken on 12 March 2013. The black dots represent the 24 h averaged position of the buoy during the period 30 November 2010 through 09 March 2011. The buoy was deployed at 38.5°S, 30.0°E (first black dot).

Physical situations which possess an infinite Lagrangian correlation time τ^* , however, correspond to superdiffusive transport. In other words, if the large-scale components of the velocity field are strong enough to move a particle (or a drifter) in the same direction for an arbitrarily long period, the resulting mean square displacement grows as a power of t : $\langle \Delta \mathcal{R}^2(t) \rangle \propto t^\alpha$ [18,19]. Specifically, when an ensemble of particles is advected by the fluid velocity, the mean square interparticle distance scales as $\langle \Delta \mathcal{R}^2(t) \rangle \propto t^3$ [20].

On the other hand, the results obtained from numerical simulations and experiments of particle dispersion on the fluid surface differs significantly from Richardson's scaling t^3 [21]. This discrepancy is presumably related to compressible flow effects of the floating-particle system. It can be seen that in the case of compressible flow the scaling ranges from $\langle \Delta \mathcal{R}^2(t) \rangle \propto t^2$ to $\langle \Delta \mathcal{R}^2(t) \rangle \propto t^{1.65}$, while at mesoscale oceanic turbulence it has been found $\langle \Delta \mathcal{R}^2(t) \rangle \propto t^{2.2}$, since the drifter motion is subject to this compressible flow [21,22].

SST data measured by the buoy are shown in Fig. 2. It is evident that, due to the particular currents in this region, frequent abrupt changes in SST can be observed, due to the strong mixing of currents with different temperatures.

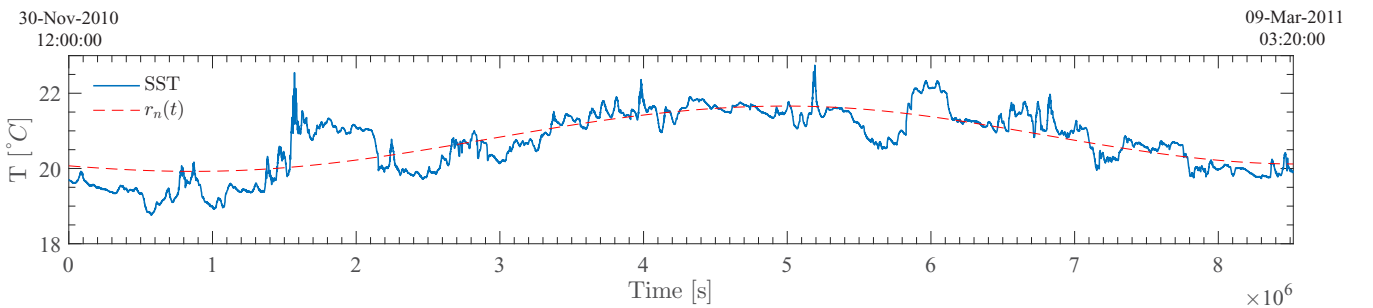


FIG. 2. Solid line: sea surface temperature measured in the period 30 November 2010 through 09 March 2011 with a sampling time $\Delta t = 600$ s. Dashed line: residual $r_n(t)$ obtained through the EMD decomposition related to the annual temperature cycle in the Agulhas current [23].

It is customary in turbulence studies to obtain information concerning the scaling properties of a turbulent scalar field $T(t)$ by investigating the scaling exponents of the structure functions, namely, the q th moments of the fluctuations $S_q = \langle [T(t + \tau) - T(t)]^q \rangle$ at a given scale τ ($\langle \cdot \rangle$ brackets represent the time average) [4,24,25]. Kolmogorov's second similarity hypothesis suggests the scaling law of the Lagrangian second-order structure function in the inertial range is $S_2(\tau) = C_0 \epsilon_0 \tau$ (for a velocity trajectory), where C_0 is a constant and ϵ_0 is the average dissipation rate. For a passive scalar, the Lagrangian scaling relation for a second-order structure function, in the inertial range, is expressed as $S_2(\tau) \propto \bar{\chi} \tau$, where $\bar{\chi}$ is the dissipation of the passive scalar variance, which is assumed to be homogeneous [26]. The intermittency effects can be introduced under the assumption of a Lagrangian cascade for the passive scalar flux: $\chi_\tau \propto \Delta T^2 / \tau$ [27,28]. The average value $\langle \chi_\tau \rangle$ is conserved by the equations of motion ($\langle \chi_\tau \rangle = \bar{\chi} = \Theta_k$, Θ_k being a constant) [29].

By defining the energy spectral density $E(\omega)$ through

$$S_2(\tau) = \int_0^\infty E(\omega) [1 - \cos(2\pi\omega\tau)] d\omega \quad (1)$$

($\omega \sim 1/\tau$), the $K41$ scaling law $S_2 \sim \tau^{\beta-1}$ results in $E(\omega) \sim \omega^{-\beta}$ ($\beta = 2$ in this case). However, experimental and numerical results [30–35] suggest that scaling behavior is anomalous with respect to the Kolmogorov phenomenology [1,2,4]. This seems to be a universal characteristic of turbulent flows, being observed also in complex fluids, such as turbulent astrophysical flows [36], charged particle flows, and anisotropic molecular flows [37,38].

The classical second-order structure function $S_2(\tau)$ can be easily calculated from the SST dataset, and is shown in Fig. 3, where a linear scaling is observed in a range of τ (open symbols) compatible with the frequency range observed in the power spectrum (Fig. 4), however, the scaling exponent is far from being comparable with $K41$, since the slope is $S_2 \sim \tau^{3/2}$, rather than the $K41$ exponent reported above.

According to [39] this discrepancy should be related to the presence of large-scale structures in the field. In the present case it is known that, on the mesoscale, oceanic SST is constantly forced by the daily solar radiation cycle, which influences CO_2 fluxes [40], latent heat flux [41], and convection [42]. This represents a particular case, inasmuch as structure functions should be used to investigate the scaling

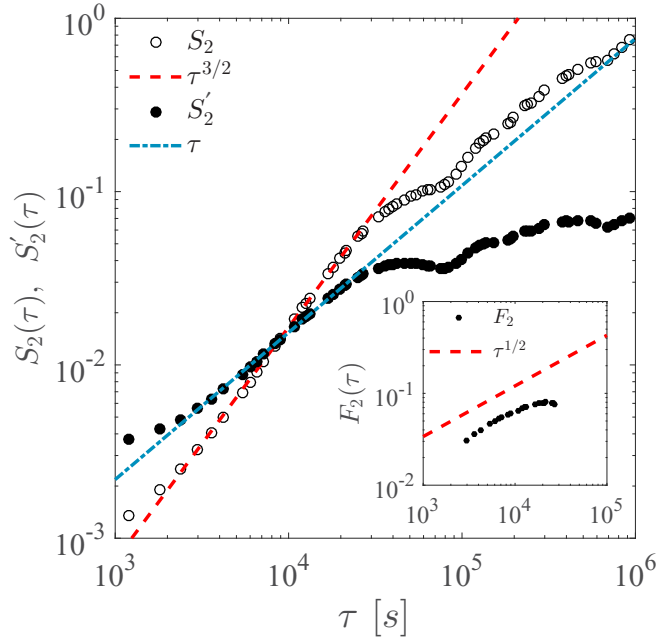


FIG. 3. Second-order structure functions $S_2(\tau)$ (open circles) and $S'_2(\tau)$ (solid circles), as a function of the scale τ . The scalings $\tau^{3/2}$ (dashed line) and τ (dash-dotted line) are reported for reference.

properties of turbulence. In fact, experiments on passive scalar transport in fluid flows, and also numerical simulations, have shown that this method may fail in the presence of large-scale periodic forcing, because the fluctuations in the inertial range can be affected over almost two orders of magnitude by large energetic structures within the dynamics [39,43,44]. In fact, the large-scale region of $S_2(\tau) \geq 5 \times 10^{-4}$ s seems to follow a different scaling. This implies that the large scales are

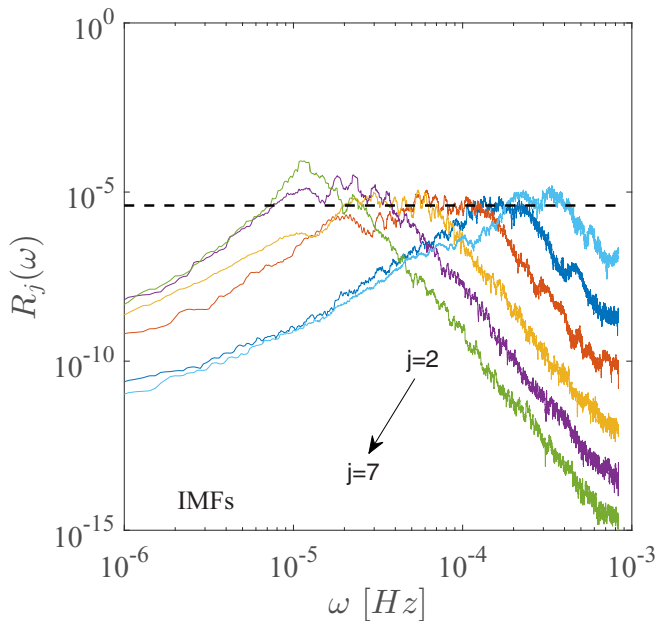


FIG. 4. Compensated power spectrum $R_j(\omega) = \Theta_j(\omega)\omega^2$ as a function of the frequency ω , for $j = 2, 3, \dots, 7$. The horizontal dashed line, reported for reference, indicates the range where $\hat{\Theta}_j(\omega) \sim \omega^{-2}$.

still correlated and possibly affect the smallest ones. The same behavior is observed for all q orders of the scaling exponents extracted from the structure function.

Therefore, to correctly extract scaling information from the ARC SST data, by minimizing the effect of the forcing, arbitrary order Hilbert spectral analysis (HSA) has been used [39,43]. HSA formally represents an extension of classical empirical mode decomposition (EMD), designed to characterize scale invariant properties directly in amplitude-frequency space [39]. EMD itself was developed to process nonstationary data [45], and has successfully been applied in many different contexts [46–49]. To apply HSA, the ARC SST data was initially decomposed through classical EMD to obtain the intrinsic mode functions (IMFs), and the Hilbert transform was then applied to the IMFs.

Within the EMD framework [45], the SST data $T(t)$ can be decomposed into a finite number n of oscillating basis functions $\Theta_j(t)$, the so-called IMFs, and a residual $r_n(t)$ which describes the mean trend, if one exists, as

$$T(t) = \sum_{j=1}^n \Theta_j(t) + r_n(t).$$

Since EMD acts intrinsically as a dyadic filter bank [50,51], each IMF captures a narrow ω band in frequency space, and their superposition behaves as $M_\Theta(\omega) \equiv \text{Max}[\hat{\Theta}_j(\omega)] \sim \omega^{-\beta}$ in the inertial range [43]. A range of frequencies where a power-law behavior can be observed is chosen (Fig. 4).

The subset of IMFs $j \in [2-7]$ is enough to capture the complete dynamics involved in the turbulent cascade process. A simple linear least squares fit of $M_\Theta(\omega)$ gives $\beta \simeq 2$ (with a reduced $\chi^2 = 0.98$) for frequencies in the range $\omega \in [2 \times 10^{-5} - 5 \times 10^{-4}]$ Hz. Figure 4 illustrates the compensated contribution $R_j(\omega) = \hat{\Theta}_j(\omega)\omega^2$ of each IMF between $j \in [2-7]$. This scaling is very similar to that obtained from laboratory measurements, where the temperature spectrum mimics the slope of the kinetic energy fluctuation [52,53].

The peak at $\omega \simeq 10^{-5}$ Hz in Fig. 4 is the daily radiation cycle forcing. The annual temperature cycle of the Agulhas current [23] is captured from the residual $r_n(t)$ (Fig. 2). The maximum of the cycle is observed in December and January.

Once the IMFs have been obtained, a Hilbert transform is performed on each:

$$\Theta_j^*(t) = \frac{P}{\pi} \int \frac{\Theta_j(t')}{t-t'} dt', \quad (2)$$

where P is the Cauchy principal value and the instantaneous frequency is given by

$$\omega_j(t) = \frac{1}{2\pi} \frac{d}{dt} \arctan \left[\frac{\Theta_j^*(t)}{\Theta_j(t)} \right]. \quad (3)$$

A joint probability density function $P(\omega, \mathcal{A})$ is obtained, related to the instantaneous frequency ω_j and the amplitude \mathcal{A}_j of the j th IMF. A marginal integration of $P(\omega, \mathcal{A})$ defines the so-called Hilbert marginal spectrum. To investigate the amplitude of turbulent temperature fluctuations versus their characteristic frequency, the ω -dependent q -order statistical moment $\mathcal{L}_q(\omega)$ was obtained by evaluating the moments of each IMF at those points where the corresponding

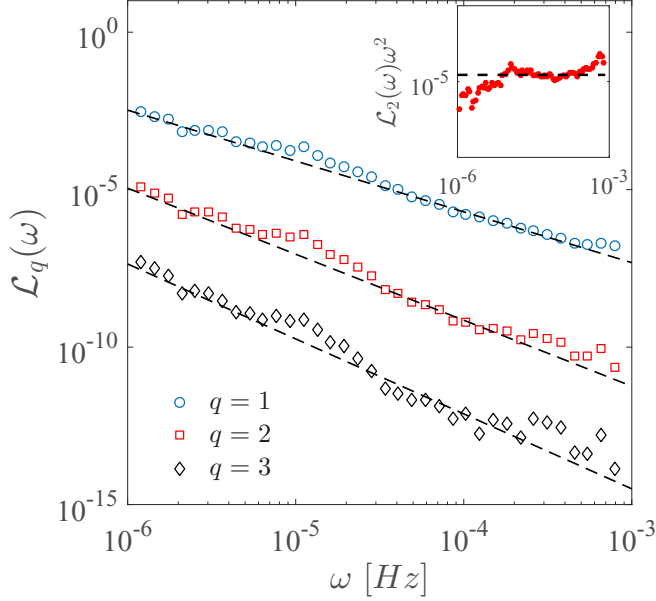


FIG. 5. The Hilbert spectra $\mathcal{L}_q(\omega)$ for $q = 1, 2, 3$. The curves have been shifted for clarity. Dashed lines represent the least squares fit.

instantaneous frequency is fixed at the value $\omega_j(t) = \omega$ [44]:

$$\mathcal{L}_q(\omega) \equiv \sum_{j=1}^n \langle |\Theta_j|^q | \omega \rangle, \quad (4)$$

where q is the order, and $\langle \cdot \rangle$ represents the time average.

Figure 5 shows the first three $\mathcal{L}_q(\omega)$ orders ($q = 1, 2, 3$) obtained from Eq. (4). The resulting $\mathcal{L}_q(\omega)$ show a clear scaling behavior $\mathcal{L}_q(\omega) \sim \omega^{-\gamma_q}$. The inset in Fig. 5 illustrates the second-order $\mathcal{L}_2(\omega)$ in compensated form, $\mathcal{L}_2(\omega)\omega^2$, thus showing that the second-order function behaves as $\mathcal{L}_2 \sim \omega^{-2}$ in the range of frequencies $\omega \in [2 \times 10^{-5} - 5 \times 10^{-4}]$ Hz (linear least squares fit, $\chi^2 \simeq 0.99$).

The scaling exponents $\xi_\Theta(q) = \gamma_q - 1$ (which are analogous to the classical exponents ζ_q obtained through the structure functions), are shown in Fig. 6. The same figure shows a comparison of $\xi_\Theta(q)$ with some other scaling exponents from the literature. It is easily observed that the departure from $K41$ scaling is fully captured by the ARC mesoscale turbulence and, furthermore, the exponents $\xi_\Theta(q)$ are surprisingly similar to the exponents obtained through the multifractal prediction in the Lagrangian frame for the velocity trajectory [44,54–56]. As can be seen in Fig. 6, the scaling exponents evaluated through the HSA are closer to that obtained from single particle statistics [44] than the exponents obtained from multiple particle dispersion [55].

This result shows that, once HSA is used, the large-scale contribution can be properly constrained. Rather unexpectedly the Lagrangian scaling properties for velocity and passive scalars are more similar than might be imagined. Within a Eulerian framework passive scalars exhibit a stronger intermittency than velocity fluctuations [16,19]. The links between scaling exponents in Eulerian and Lagrangian frameworks have been described by [16]. However, superposition of the passive scalar and velocity fluctuation scaling has been obtained in the Eulerian case when HSA has been performed on laboratory

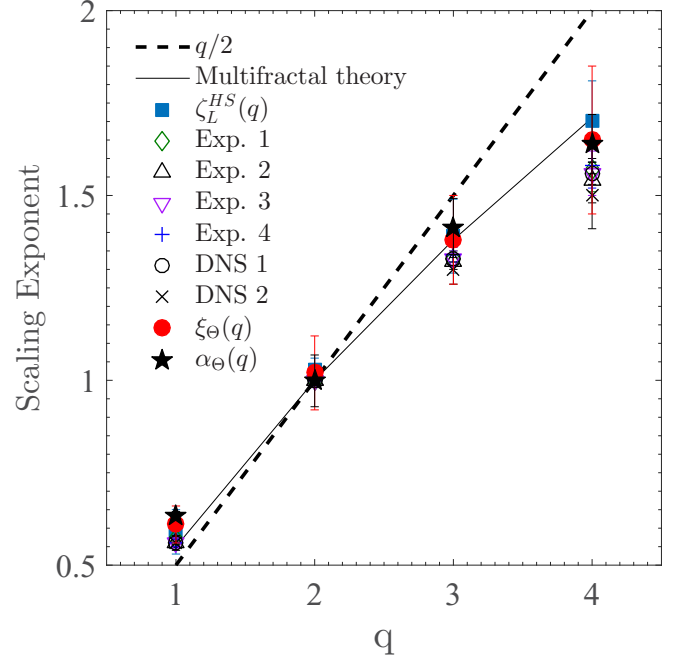


FIG. 6. Comparison of the scaling exponent obtained for velocity and temperature data: $\zeta_L^{HS}(q)$ multifractal scaling exponents for single particle velocity trajectories [44]. Exp. 1, Exp. 2, Exp. 3, Exp. 4: scaling exponent for multiple particle dispersion from [55], at different Reynolds number $Re = 510, 570, 810, 1000$, respectively. DNS 1 and DNS 2: scaling exponent from numerical simulation of multiple particle dispersion from [55], at $Re = 75, 140$, with 5000 and 10 000 particles, respectively. $\xi_\Theta(q)$: scaling exponent for ARC-SST obtained through the HSA. $\alpha_\Theta(q)$: scaling exponent evaluated from renormalized structure function for ARC-SST. Dashed line ($K41, q/2$): Lagrangian scaling exponents as estimated from dimensional analysis [24]. Solid line: multifractal theory [56].

temperature data [39]. It was shown that when the large-scale contribution of the velocity field is properly constrained, the scaling exponents for passive scalars are comparable to those obtained from ESS for velocity fluctuations [39].

In order to check the correctness of the result obtained through the HSA, the scaling exponent of the ARC-SST has been recovered using an alternative approach. Consider Eq. (1), which defines $S_2(\tau)$ in terms of the spectral energy density. The effect of large scales on the smallest ones can be estimated by introducing the function $F(\tau) \simeq [S_2(\tau)]^{-1} I(\tau)$, where

$$I(\tau) = \int_0^{\omega_1} E(\omega) [1 - \cos(2\pi\omega\tau)] d\omega. \quad (5)$$

The value ω_1 represents the high-frequency boundary of the large scales, in this case $\omega_1 \simeq 10^{-5}$. A new second-order structure function, which should be roughly unaffected by the large scales, can be estimated through $S'_2(\tau) = S_2(\tau)/F(\tau)$. Using the spectral density $E(\omega)$ previously calculated in Eq. (5), a simple numerical integration gives $F(\tau) \sim \tau^{1/2}$, as shown in the inset of Fig. 3. The plot of $S'_2(\tau)$ in Fig. 3 shows the corrected scaling law for the second-order structure function. A correction to the whole set of q th-order structure functions may be postulated, as an order of magnitude estimate, by the

rescaling

$$S'_q(\tau) = [S_q(\tau)]^2 I^{-q/2}. \quad (6)$$

The scaling exponents of S'_q calculated through $S'_q \sim \tau^{\alpha_q}$ are shown in Fig. 6. Thus even without using HSA, a phenomenological renormalization of structure functions yields a scaling behavior similar to the multifractal scaling obtained for velocity fluctuation (single particle case) [44,56].

In summary, the Lagrangian statistics of the SST in the ARC, a mesoscale oceanic environment, has been investigated. The influence of the largest scales over the inertial range has been avoided using arbitrary order HSA, and the correct scalings of the higher-order moments of the Lagrangian temperature fluctuations has been obtained from the Hilbert marginal spectrum.

In particular, we found that (i) the scaling exponents for the ARC-SST are strictly comparable to those of the velocity trajectory obtained from the multifractal prediction once the effects of the largest scales are properly constrained and (ii) the spectral behavior of the Lagrangian ARC-SST turbulence, which shows a classical departure from the Kolmogorov theory, is fully compatible with the results obtained from laboratory experiments, even though the scales are completely different. Finally, the possibility of a phenomenological renormalization of the structure functions is discussed in situations where the scale separation is not fulfilled due to the influence of the large scales over the inertial range.

To conclude, this may be interpreted as the fingerprint of a possible universality between the scaling of the q th-order moment of velocity and temperature, and is in agreement with similar results obtained for the Eulerian case [39]. However, before claiming universality more studies should be conducted.

-
- [1] A. N. Kolmogorov, C. R. (Dokl.) Acad. Sci. URSS **30**, 301 (1941).
- [2] A. N. Kolmogorov, *Proc. R. Soc. London A* **434**, 9 (1991).
- [3] W. McComb, *The Physics of Fluid Turbulence* (Oxford University Press, New York, 1990).
- [4] U. Frish, *Turbulence: The legacy of A. N. Kolmogorov* (Cambridge University Press, Cambridge, UK, 1995).
- [5] C. S. Willett, R. R. Leben, and M. F. Lavn, *Prog. Oceanogr.* **69**, 218 (2006).
- [6] R.-C. Lien, E. A. D'Asaro, and C. E. Menkes, *Geophys. Res. Lett.* **35** (2008).
- [7] J. Skákala and T. J. Smyth, *J. Geophys. Res.: Oceans* **120**, 6253 (2015).
- [8] P. K. Yeung, *Annu. Rev. Fluid Mech.* **34**, 115 (2002).
- [9] O. Boebel, T. Rossby, J. Lutjeharms, W. Zenk, and C. Barron, *Deep Sea Res., Part II* **50**, 35 (2003).
- [10] L. M. Beal, W. P. M. De Ruijter, A. Biastoch, and R. Zahn, *Nature (London)* **472**, 429 (2011).
- [11] See <http://www.pmel.noaa.gov/ocs/>.
- [12] See <http://www.pmel.noaa.gov/ocs/ARC>.
- [13] P. P. Niiler, A. S. Sybrandy, K. Bi, P. M. Poulain, and D. Bitterman, *Deep Sea Res., Part I* **42**, 1951 (1995).
- [14] P. Falco, A. Griffa, P. M. Poulain, and E. Zambianchi, *J. Phys. Oceanogr.* **30**, 2055 (2000).
- [15] P. M. Poulain, *J. Marine Syst.* **29**, 3 (2001).
- [16] F. G. Schmitt, *Eur. Phys. J. B* **48**, 129 (2005).
- [17] G. I. Taylor, *Proc. London Math. Soc.* **s2-20**, 196 (1922).
- [18] G. Matheron and G. De Marsily, *Water Resour. Res.* **16**, 901 (1980).
- [19] G. Falkovich, K. Gawędzki, and M. Vergassola, *Rev. Mod. Phys.* **73**, 913 (2001).
- [20] L. F. Richardson, *Proc. R. Soc. London, Ser. A* **110**, 709 (1926).
- [21] J. R. Cressman, J. Davoudi, W. I. Goldberg, and J. Schumacher, *New J. Phys.* **6**, 53 (2004).
- [22] J. H. LaCasce and O. Carter, *J. Mar. Res.* **61**, 285 (2003).
- [23] M. Krug and J. Tournadre, *Geophys. Res. Lett.* **39**, L15607 (2012).
- [24] A. S. Monin and A. M. Yaglom, *Statistical Fluid Mechanics: Mechanics of Turbulence* (Dover, New York, 2007).
- [25] D. Lohse and K.-Q. Xia, *Annu. Rev. Fluid Mech.* **42**, 335 (2010).
- [26] E. Inoue, *J. Meteorol. Soc. Jpn., Ser. II* **30**, 289 (1952).
- [27] E. A. Novikov, *Phys. Fluids A* **1**, 326 (1989).
- [28] E. A. Novikov, *Phys. Fluids A* **2**, 814 (1990).
- [29] L. Seuront and F. G. Schmitt, *Geophys. Res. Lett.* **31** (2004).
- [30] K. Sreenivasan, *J. Fluid Mech.* **151**, 81 (1985).
- [31] K. Sreenivasan, *Annu. Rev. Fluid Mech.* **29**, 435 (1997).
- [32] F. Anselmet, Y. Gagne, E. J. Hopfinger, and R. A. Antonia, *J. Fluid Mech.* **140**, 63 (1984).
- [33] A. Arneodo *et al.*, *Europhys. Lett.* **34**, 411 (1996).
- [34] M. M. A. Vincent, *J. Fluid Mech.* **225**, 1 (1991).
- [35] O. N. Boratav and R. B. Pelz, *Phys. Fluids* **9**, 1400 (1997).
- [36] R. Bruno and V. Carbone, *Living Rev. Sol. Phys.* **2**, 4 (2005).
- [37] E. Leonardis, L. Sorriso-Valvo, F. Valentini, S. Servidio, F. Carbone, and P. Veltri, *Phys. Plasmas* **23**, 022307 (2016).
- [38] F. Carbone and L. Sorriso-Valvo, *Eur. Phys. J. E* **37**, 1 (2014).
- [39] Y. X. Huang, F. G. Schmitt, Z. M. Lu, P. Fougairolles, Y. Gagne, and Y. L. Liu, *Phys. Rev. E* **82**, 026319 (2010).
- [40] H. Kettle, C. J. Merchant, C. D. Jeffery, M. J. Filipiak, and C. L. Gentemann, *Atmos. Chem. Phys.* **9**, 529 (2009).
- [41] H. Seo, A. C. Subramanian, A. J. Miller, and N. R. Cavanaugh, *J. Climate* **27**, 8422 (2014).
- [42] C. A. Clayson and D. Weitlich, *J. Climate* **20**, 334 (2007).
- [43] Y. X. Huang, F. G. Schmitt, Z. M. Lu, and Y. L. Liu, *Europhys. Lett.* **84**, 40010 (2008).
- [44] Y. Huang, L. Biferale, E. Calzavarini, C. Sun, and F. Toschi, *Phys. Rev. E* **87**, 041003 (2013).
- [45] N. E. Huang, Z. Shen, S. R. Long, M. C. Wu, H. H. Shih, Q. Zheng, N.-C. Yen, C. C. Tung, and H. H. Liu, *Proc. R. Soc. London, Ser. A* **454**, 903 (1998).
- [46] J. I. Salisbury and M. Wimbush, *Nonlin. Processes Geophys.* **9**, 341 (2002).
- [47] Z. Wu, E. K. Schneider, B. P. Kirtman, E. S. Sarachik, N. E. Huang, and C. J. Tucker, *Climate Dynam.* **31**, 823 (2008).
- [48] A. Vecchio, M. Anzidei, and V. Carbone, *J. Geodynam.* **79**, 39 (2014).

- [49] F. Carbone, M. S. Landis, C. N. Gencarelli, A. Naccarato, F. Sprovieri, F. De Simone, I. M. Hedgecock, and N. Pirrone, *Geophys. Res. Lett.* **43**, 7751 (2016).
- [50] P. Flandrin, G. Rilling, and P. Goncalves, *IEEE Signal Process. Lett.* **11**, 112 (2004).
- [51] *The Hilbert-Huang Transform and Its Applications*, edited by N. E. Huang and S. S. P. Shen (World Scientific, Singapore, 2005).
- [52] Y. Gasteuil, W. L. Shew, M. Gibert, F. Chillá, B. Castaing, and J.-F. Pinton, *Phys. Rev. Lett.* **99**, 234302 (2007).
- [53] O. Liot, F. Seychelles, F. Zonta, S. Chibbaro, T. Coudarchet, Y. Gasteuil, J.-F. Pinton, J. Salort, and F. Chillá, *J. Fluid Mech.* **794**, 655 (2016).
- [54] L. Chevillard, S. G. Roux, E. Levêque, N. Mordant, J.-F. Pinton, and A. Arneodo, *Phys. Rev. Lett.* **91**, 214502 (2003).
- [55] N. Mordant, E. Lvque, and J.-F. Pinton, *New J. Phys.* **6**, 116 (2004).
- [56] L. Biferale, G. Boffetta, A. Celani, B. J. Devenish, A. Lanotte, and F. Toschi, *Phys. Rev. Lett.* **93**, 064502 (2004).